

Magnetic reconnection with asymmetry in the outflow direction

N. A. Murphy,^{1,2,3} C. R. Sovinec,^{1,4} and P. A. Cassak⁵

Received 9 December 2009; revised 23 March 2010; accepted 11 May 2010; published 4 September 2010.

[1] Magnetic reconnection with asymmetry in the outflow direction occurs in the Earth's magnetotail, coronal mass ejections, flux cancellation events, astrophysical disks, spheromak merging experiments, and elsewhere in nature and the laboratory. A control volume analysis is performed for the case of steady antiparallel magnetic reconnection with asymmetric downstream pressure to derive scaling relations for the outflow velocity from each side of the current sheet and the reconnection rate. Simple relationships for outflow velocity are presented for the incompressible case and the case of symmetric downstream pressure but asymmetric downstream density. Asymmetry alone is not found to greatly affect the reconnection rate. The flow stagnation point and magnetic field null do not coincide in a steady state unless the pressure gradient is negligible at the flow stagnation point. The predictions of the model are compared with resistive MHD simulations of driven reconnection with asymmetry in the outflow direction.

Citation: Murphy, N. A., C. R. Sovinec, and P. A. Cassak (2010), Magnetic reconnection with asymmetry in the outflow direction, *J. Geophys. Res.*, 115, A09206, doi:10.1029/2009JA015183.

1. Introduction

[2] While most two-dimensional models of magnetic reconnection assume that the process is symmetric to a 180° rotation about the X-point, there are many situations in nature and in the laboratory where this assumption is invalid. In recent years, many papers have addressed magnetic reconnection with asymmetry in the inflow direction [e.g., *La Belle-Hamer et al.*, 1995; *Nakamura and Scholer*, 2000; *Swisdak et al.*, 2003; *Øieroset et al.*, 2004; *Borovsky and Hesse*, 2007; *Cassak and Shay*, 2007, 2008, 2009; *Birn et al.*, 2008; *Murphy and Sovinec*, 2008; *Mozer et al.*, 2008; *Pritchett*, 2008; *Borovsky et al.*, 2008; *Tanaka et al.*, 2008; *Mozer and Pritchett*, 2009; *Eriksson et al.*, 2009]. In particular, *Cassak and Shay* [2007] generalized the Sweet-Parker model [*Parker*, 1957, 1963; *Sweet*, 1958] to account for reconnection between plasmas with different upstream densities and magnetic field strengths. They found that the reconnection rate is governed by a hybrid Alfvén speed that takes into account the densities and magnetic field strengths for the two upstream regions. The positions of the magnetic field null and flow stagnation point are displaced from each other, with the field null position set by balance of energy

flux and the stagnation point position set by balance of mass flux. In addition to reconnection with asymmetric inflow, there are many situations in nature and the laboratory for which the outflow rather than the inflow is asymmetric. In this paper, we analyze steady magnetic reconnection with asymmetry in the outflow direction.

[3] The best known scenario for magnetic reconnection with asymmetry in the outflow direction is the Earth's magnetotail. In this case, asymmetry is a particularly important consideration because it helps determine the amount of energy transported in the earthward and tailward directions as a result of reconnection. At distances of ~5–15 R_E , there is a considerable pressure gradient as the plasma pressure decreases approximately monotonically with distance from Earth [*Lui et al.*, 1994; *Shiokawa et al.*, 1997; *Xing et al.*, 2010]. Earthward-directed reconnection outflow must work against strong gradients in both plasma pressure and magnetic pressure. Because of the global configuration of the magnetotail and its response to reconnection, the X-line characteristically moves in the tailward direction [e.g., *Runov et al.*, 2003]. Reconnection with asymmetry in the outflow direction has often been seen in simulations of the magnetotail [e.g., *Birn et al.*, 1996; *Hesse et al.*, 1996; *Hesse and Schindler*, 2001; *Kuznetsova et al.*, 2007; *Laitinen et al.*, 2005; *Laitinen*, 2007; *Birn and Hesse*, 2009; *Zhu et al.*, 2009], though the degree of asymmetry depends on the proximity of the reconnection layer to Earth and how reconnection is driven.

[4] In solar physics, reconnection during coronal mass ejections (CMEs), solar flares, and flux cancellation events are asymmetric in the outflow direction when one outflow jet propagates sunward into a high density region and the other outflow jet propagates antisunward into a low density region or a rising plasmoid [e.g., *Kopp and Pneuman*, 1976; *Martin et al.*, 1985; *Shibata et al.*, 1995; *Litvinenko*, 1999;

¹Center for Magnetic Self-Organization in Laboratory and Astrophysical Plasmas, University of Wisconsin–Madison, Madison, Wisconsin, USA.

²Department of Astronomy, University of Wisconsin–Madison, Madison, Wisconsin, USA.

³Now at Harvard-Smithsonian Center for Astrophysics, Cambridge, Massachusetts, USA.

⁴Department of Engineering Physics, University of Wisconsin–Madison, Madison, Wisconsin, USA.

⁵Department of Physics, West Virginia University, Morgantown, West Virginia, USA.

Lin and Forbes, 2000; Aurass et al., 2002]. Observations of bidirectional jets in the solar atmosphere [see *Innes et al., 1997; Wang et al., 2007; Liu et al., 2009; Gontikakis et al., 2009*] show that, despite the effects of gravity, the redshifted jet is often slower than the blueshifted jet because the redshifted jet must propagate into a higher density medium. In these events, gravity's most important effect is the establishment of a stratified medium. Current sheets forming in such a medium are likely to have strong gradients in the outflow direction for upstream density, pressure, and magnetic field strength [see *Ciaravella et al., 2002; Ko et al., 2003; Chen et al., 2004; Bemporad et al., 2006; Lin et al., 2007, 2009; Ciaravella and Raymond, 2008; Bemporad, 2008; Vršnak et al., 2009; Saint-Hilaire et al., 2009; Aurass et al., 2009; Schettino et al., 2010*]. *Seaton [2008]* predicts that antisunward outflow from CME current sheets should be much quicker than the sunward outflow and that the predominant X-line should be near the lower tip of the current sheet. Simulations of reconnection in a stratified medium show that the redshifted jet can be up to an order of magnitude slower than the blueshifted jet [*Roussev et al., 2001*], and that reconnection in such an atmosphere displays a more complicated velocity structure than symmetric two-dimensional reconnection [*Galsgaard and Roussev, 2002*]. Gravity itself can be an important consideration if the work done by electromagnetic forces is comparable to or less than the work done by gravity [*Reeves, 2006*]. Asymmetry in the outflow direction also happens when magnetic field lines in one downstream region are line-tied while magnetic field lines in the other downstream region are open.

[5] During turbulent reconnection [e.g., *Lazarian and Vishniac, 1999*] and reconnection occurring during a turbulent cascade [e.g., *Servidio et al., 2009*], there will in general be many reconnection sites throughout the volume of interest. Reconnection occurring at each of these sites will in general be asymmetric in the inflow and outflow directions, as well as the out-of-plane direction. Reconnection processes involving multiple competing reconnection sites or multiple magnetic islands [e.g., *Lee and Fu, 1986; Drake et al., 2006; J. Lin et al., 2008; Chen et al., 2009; Nakamura et al., 2010*] will also likely involve asymmetry in the outflow direction, especially if the X-lines are not evenly spaced or develop at different rates.

[6] In astrophysical settings, the winds of strongly magnetized hot stars (e.g., the Bp star σ Ori E) can be channeled along a predominantly dipolar field to form an equatorial circumstellar disk or buildup of material [*Nakajima, 1985; Cassinelli et al., 2002; Townsend and Owocki, 2005*]. While the dipole field is in general dominant close to the star, recent axisymmetric simulations showed that the continual funneling of material can eventually lead to centrifugal breakout events associated with magnetic reconnection [*ud-Doula et al., 2006, 2008*]. In this case, the reconnection outflow is aligned with the radial direction, with one exhaust path directed towards the disk and the star and the other leading to the interstellar medium.

[7] In the laboratory, reconnection with asymmetry in the outflow direction occurs during the merging of spheromaks and in toroidal plasma configurations where the reconnection outflow is aligned with the radial direction. Relevant experiments include the Swarthmore Spheromak Experiment (SSX) [*Cothran et al., 2003*], the Magnetic Reconnection

Experiment (MRX) [*Yamada et al., 1997*], and TS-3/4 at the University of Tokyo [*Ono et al., 1993*]. Recent spheromak merging experiments at MRX have shown that asymmetry in the outflow direction develops as a result of the Hall effect [*Inomoto et al., 2006; Murphy and Sovinec, 2008*]. Hybrid simulations of spheromak merging in SSX show reconnection with much stronger radially inward directed outflow [*Y. Lin et al., 2008*]. These results suggest that considerations of asymmetry in the outflow direction are important for the interpretation of bidirectional jets recently reported in experiment [*Brown et al., 2006*].

[8] *Murphy and Sovinec [2008]* presented simulations of the reconnection process in the geometry of MRX, showing that asymmetric inflow occurs during the pull mode of operation and asymmetric outflow occurs during the push mode of operation [see *Yamada et al., 1997, Figure 3*]. The inboard (low radius) side of the current sheet is more susceptible to buildup or depletion of density due to the lesser available volume than on the outboard (high radius) side of the current sheet. As a result of the pressure buildup at low radii during push reconnection, the X-point is located closer to the outboard side of the current sheet than the inboard side. Consequently, the radially inward directed outflow is subjected to a stronger tension force than the radially outward directed outflow, allowing comparable outflow velocities from both the inboard and outboard sides of the current sheet (a similar effect is discussed by *Galsgaard and Roussev [2002]*). During several time intervals in these simulations and despite the higher pressure in the inboard downstream region, the radially inward directed outflow speed is found to be greater than the radially outward directed outflow speed. The magnetic field null and flow stagnation point are separated during both pull and push reconnection [*Murphy, 2009, Figures 2.4 and 2.6*]. Push reconnection is an example of how asymmetry in the outflow direction develops when outflow in one downstream region is confined more effectively than outflow in the other downstream region.

[9] *Oka et al. [2008]* performed particle-in-cell (PIC) simulations of reconnection where outflow from one end of the current sheet is impeded by a hard wall while outflow from the other end encounters no such obstruction. They found that the X-line retreats from the wall at $\sim 10\%$ of the upstream Alfvén velocity and that the reconnection rate is largely unchanged from the symmetric case. Moreover, there is a separation between the ion flow stagnation point and the magnetic field null, with the field null located further from the wall than the ion flow stagnation point. This simulation effort shows that current sheet motion can lead to an asymmetric outflow pattern [see also *Rogers and Zakharov, 1995; Swisdak et al., 2003; Owen and Cowley, 1987a, 1987b; Kiehas et al., 2007, 2009*].

[10] In this paper, we perform a control volume analysis for a current sheet with asymmetric downstream pressure and test the resulting scaling relations against simulations. The objectives are to determine (1) the relationship between the upstream parameters, the downstream pressures, and the reconnection outflow velocity, (2) how the reconnection rate is affected by asymmetric downstream pressure, and (3) what sets the positions of the magnetic field null and flow stagnation point. In section 2, we write the equations of resistive magnetohydrodynamics (MHD) in a time-independent integral form that is amenable to a control

volume analysis. In section 3, we review the effects of symmetric downstream pressure on antiparallel reconnection and develop scaling relations for a current sheet with asymmetric downstream pressure. In section 4, we test the scaling relations derived in section 3 against resistive MHD simulations of reconnection with asymmetry in the outflow direction. In section 5, we provide a discussion and summarize our results. A similar analysis for reconnection in cylindrical geometry with outflow aligned with the radial direction is presented by *Murphy* [2009, section 3.4].

2. Equations of Magnetohydrodynamics

[11] The equations of resistive MHD in conservative form [e.g., *Goedbloed and Poedts*, 2004, pp. 165–166] are

$$\frac{\partial \rho}{\partial t} + \nabla \cdot (\rho \mathbf{V}) = 0, \quad (1)$$

$$\frac{\partial(\rho \mathbf{V})}{\partial t} + \nabla \cdot \left[\rho \mathbf{V} \mathbf{V} + \left(p + \frac{B^2}{2\mu_0} \right) \hat{\mathbf{i}} - \frac{\mathbf{B}\mathbf{B}}{\mu_0} \right] = 0, \quad (2)$$

$$\frac{\partial \mathcal{E}}{\partial t} + \nabla \cdot \left[\left(\frac{\rho V^2}{2} + \frac{\gamma}{\gamma-1} p \right) \mathbf{V} + \frac{\mathbf{E} \times \mathbf{B}}{\mu_0} \right] = 0, \quad (3)$$

$$\frac{\partial \mathbf{B}}{\partial t} + \nabla \times \mathbf{E} = 0, \quad (4)$$

$$\mu_0 \mathbf{J} = \nabla \times \mathbf{B}, \quad (5)$$

$$\mathbf{E} + \mathbf{V} \times \mathbf{B} = \eta \mathbf{J}, \quad (6)$$

where \mathbf{B} is the magnetic field, \mathbf{E} is the electric field, \mathbf{V} is the bulk plasma velocity, \mathbf{J} is the current density, p is the plasma pressure, ρ is mass density, η is the plasma resistivity, $\mathcal{E} \equiv \rho V^2/2 + p/(\gamma-1) + B^2/2\mu_0$ is the total energy density, and γ is the ratio of specific heats. The identity dyadic tensor is given by $\hat{\mathbf{i}} = \hat{\mathbf{x}}\hat{\mathbf{x}} + \hat{\mathbf{y}}\hat{\mathbf{y}} + \hat{\mathbf{z}}\hat{\mathbf{z}}$. Equation (3) includes the internal energy flux, $p\mathbf{V}/(\gamma-1)$, and the mechanical work done on or by the plasma by pressure gradients while moving, $p\mathbf{V}$.

[12] Following the approach presented by *Cassak and Shay* [2007], we assume a steady-state system, integrate over an arbitrary closed volume \mathcal{V} bounded by the surface \mathcal{S} , and use the divergence theorem to write the continuity, momentum, and energy equations as

$$\oint_{\mathcal{S}} d\mathbf{S} \cdot (\rho \mathbf{V}) = 0, \quad (7)$$

$$\oint_{\mathcal{S}} d\mathbf{S} \cdot \left[\rho \mathbf{V} \mathbf{V} + \left(p + \frac{B^2}{2\mu_0} \right) \hat{\mathbf{i}} - \frac{\mathbf{B}\mathbf{B}}{\mu_0} \right] = 0, \quad (8)$$

$$\oint_{\mathcal{S}} d\mathbf{S} \cdot \left[\left(\frac{\rho V^2}{2} + \frac{\gamma p}{\gamma-1} \right) \mathbf{V} + \frac{\mathbf{E} \times \mathbf{B}}{\mu_0} \right] = 0, \quad (9)$$

where $d\mathbf{S}$ is a differential area element pointing in the outward normal direction to \mathcal{S} . Similarly, with the help of Stokes' theorem, equation (4) leads to

$$\oint_{\mathcal{S}} d\mathbf{S} \times \mathbf{E} = 0. \quad (10)$$

Equations (7)–(10) are valid for any arbitrary closed volume, provided a steady-state has been achieved. These surface integrals are evaluated in section 3 to investigate magnetic reconnection with asymmetry in the outflow direction.

3. Scaling Relations

[13] The Sweet-Parker model describes symmetric steady-state antiparallel magnetic reconnection in the resistive MHD framework when compressibility, viscosity, and downstream pressure are unimportant. In this section, we extend these results to account for reconnection with asymmetric downstream pressure. After reviewing the effects of symmetric downstream pressure on the reconnection process in section 3.1, we consider the case of asymmetric downstream plasma pressure in section 3.2. We then investigate the internal structure of such a current sheet in section 3.3.

3.1. Effects of Symmetric Downstream Pressure

[14] The effects of symmetric downstream pressure on a Sweet-Parker current sheet are discussed by *Priest and Forbes* [2000, pp. 123–126]. Presently, we review their results using the approach that we employ later this section for a current sheet with asymmetric downstream pressure while relaxing their assumptions regarding compressibility [see also *Parker*, 1963; *Chae et al.*, 2003; *Litvinenko and Chae*, 2009]. The characteristic parameters used in this derivation are: B_{in} , upstream magnetic field strength; V_{in} , plasma inflow velocity; V_{out} , plasma outflow velocity; p_{in} , upstream plasma pressure; p_{out} , downstream plasma pressure; ρ_{in} , upstream plasma density; ρ_{out} , downstream plasma density; J_y , out-of-plane current density inside the layer; E_y , out-of-plane electric field; L , current sheet half-length; and δ , current sheet half-thickness. We define x as the outflow direction, y as the direction into the plane, and z as the inflow direction.

[15] Everywhere except within the reconnection layer, the ideal Ohm's law is approximately valid. By assuming a steady state the electric field is constant and given by

$$E_y = V_{in} B_{in}. \quad (11)$$

Since B_x reverses over a distance of $\sim 2\delta$, Ampere's law gives

$$J_y \sim \frac{B_{in}}{\mu_0 \delta}. \quad (12)$$

Matching the resistive electric field inside the layer with the ideal electric field outside the layer gives

$$V_{in} \sim \frac{\eta}{\mu_0 \delta}. \quad (13)$$

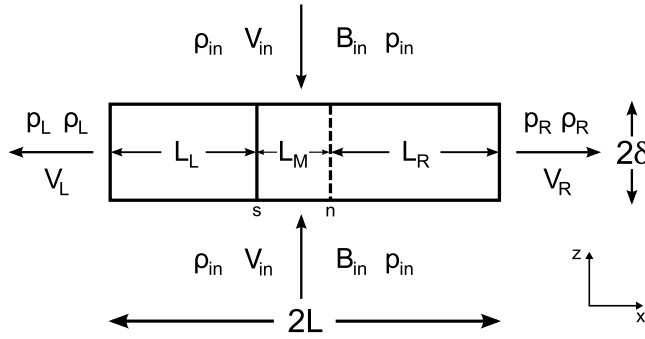


Figure 1. Sweet-Parker-like reconnection with asymmetric downstream pressure and a pressure gradient through the current sheet. The solid vertical bar inside the current sheet (marked ‘s’) represents the flow stagnation point and the dashed vertical bar (marked ‘n’) represents the magnetic field null.

[16] Evaluating the conservation of mass relation given in equation (7) over the entire volume of the current sheet yields the relation

$$\rho_{in} V_{in} L \sim \rho_{out} V_{out} \delta. \quad (14)$$

[17] The conservation of momentum surface integral given in equation (8) is satisfied by any distribution of fluxes with the assumed symmetry when integrating over the outer boundary of the current sheet. Evaluating the conservation of energy relation given in equation (9) yields the relation

$$V_{in} L \left(\alpha p_{in} + \frac{B_{in}^2}{\mu_0} \right) \sim V_{out} \delta \left(\alpha p_{out} + \frac{\rho_{out} V_{out}^2}{2} \right), \quad (15)$$

where $\alpha \equiv \gamma/(\gamma - 1)$. Assuming $\delta \ll L$, the upstream kinetic energy and downstream Poynting flux can be neglected because they are second order small in powers of δ/L . Dividing equation (15) by equation (14) and rearranging gives the scaling relation

$$V_{out}^2 \sim V_A^2 - \alpha \left(\frac{p_{out}}{\rho_{out}} - \frac{p_{in}}{\rho_{in}} \right), \quad (16)$$

where $V_A \equiv B_{in}/\sqrt{\mu_0 \rho_{in}}$ is the upstream Alfvén speed and we ignore factors of order unity. This reduces to equation (4.26) of *Priest and Forbes* [2000] to within a factor of two. The term $\alpha p/\rho$ is the enthalpy per unit mass. Using equation (13), the scaling for the dimensionless reconnection rate can then be written as

$$\frac{V_{in}}{V_A} \sim \frac{1}{S^{1/2}} \sqrt{\frac{\rho_{out}}{\rho_{in}}} \left[1 - \frac{\alpha}{V_A^2} \left(\frac{p_{out}}{\rho_{out}} - \frac{p_{in}}{\rho_{in}} \right) \right]^{1/4} \quad (17)$$

where $S \equiv \mu_0 L V_A / \eta$ is the Lundquist number. The reconnection rate depends weakly on the downstream pressure except when the bracketed quantity is close to zero. The Sweet-Parker scalings of $V_{out} \sim V_A$ and $V_{in}/V_A \sim S^{-1/2}$ are recovered when ρ_{out}/ρ_{in} and the quantity in brackets are independent of S . We also see that when compression makes

the outflow density larger than the inflow density, it relaxes the usual bottleneck from flow moving through the reconnection region.

3.2. Effects of Asymmetric Downstream Pressure

[18] We now consider a current sheet with symmetric inflow but with asymmetric outflow and downstream pressure. In this framework, it is necessary to assume that the current sheet position and structure is steady within the inertial reference frame of the X-line. For example, reconnection could be externally driven in such a way that constrains the position of the current sheet. The setup of this problem is shown in Figure 1. Throughout this analysis, subscripts L and R indicate that the variable represents the characteristic downstream value of a field for the left and right sides of the current sheet.

[19] To proceed, we evaluate the surface integrals given in equations (7)–(9) over the whole volume of the current sheet depicted in Figure 1. The conservation of mass surface integral given in equation (7) yields the relation

$$2L \rho_{in} V_{in} \sim \rho_L V_L \delta + \rho_R V_R \delta. \quad (18)$$

We assume for simplicity that the left and right sides of the current sheet have the same thickness.

[20] Evaluating the component of the conservation of momentum surface integral given in equation (8) in the outflow direction yields a relation between the plasma pressures and momentum fluxes from each exit of the reconnection layer,

$$\rho_L V_L^2 + p_L \sim \rho_R V_R^2 + p_R. \quad (19)$$

Equation (19) assumes that the net contribution by magnetic tension towards momentum balance in the outflow direction is small. However, magnetic tension does not need to be negligible throughout the volume of integration for this relationship to hold. Rather, tension need only either be negligible along the boundary or contribute along the boundary evenly in both outflow directions. If the upstream magnetic field is not parallel to the boundaries along $z = \pm \delta$ in a way which is not symmetric in the outflow direction, tension will provide an additional contribution. For example, a nonzero net contribution from magnetic tension is expected when the predominant X-line is located near one end of the current sheet. Hence we caution that equation (19) may not include all relevant contributions. Downstream magnetic pressure is neglected because it is normally expected to be second order in powers of δ/L , but it can be important when the global magnetic field configuration contains a large vertical component that impedes outflow from one side of the current sheet [e.g., *Inomoto et al.*, 2006; *Murphy and Sovinec*, 2008]. The momentum flux $\rho \mathbf{V} \mathbf{V}$ into the current sheet is expected to significantly contribute to momentum balance in the outflow direction only when the outflow component of the inflow velocity is of the same order as the outflow velocities. Momentum balance must be met in both the inflow and outflow directions simultaneously in order for the assumption of time-independence to be valid.

[21] Using the expression for the electric field given in equation (11), the energy conservation integral (9) provides the relation

$$2LV_{in} \left(\alpha p_{in} + \frac{B_{in}^2}{\mu_0} \right) \sim V_L \delta \left(\alpha p_L + \frac{\rho_L V_L^2}{2} \right) + V_R \delta \left(\alpha p_R + \frac{\rho_R V_R^2}{2} \right). \quad (20)$$

The above relation neglects upstream kinetic energy and the Poynting flux out of the layer. As in equation (15), this is justified when $\delta \ll L$.

[22] By using equation (18) to eliminate $2LV_{in}$ from equation (20) and equation (19) to eliminate V_R , we arrive at the following cubic relationship which can be solved for V_L^2 ,

$$0 \sim C_{6L} V_L^6 + C_{4L} V_L^4 + C_{2L} V_L^2 + C_{0L}, \quad (21)$$

where we do not explicitly assume the nature of the dissipation mechanism. The coefficients for the above equation are functions of the upstream magnetic field strength as well as the upstream and downstream densities and pressures, and are given by

$$C_{6L} \equiv \frac{1}{4} \left(\frac{\rho_L^3}{\rho_R} - \rho_L^2 \right), \quad (22)$$

$$C_{4L} \equiv \frac{\rho_L^2}{\rho_R} \left(\alpha p_R - \frac{3}{4} \Delta p \right) - \alpha \rho_L p_L \quad (23)$$

$$C_{2L} \equiv \rho_L (\rho_R - \rho_L) c_{in}^4 + 2\rho_L \Delta p (1 - \alpha) c_{in}^2 - \alpha^2 p_L^2 + \alpha^2 p_R^2 \left[\frac{\rho_L}{\rho_R} \left(1 - \frac{\Delta p}{2\alpha p_R} \right) \left(1 - \frac{3\Delta p}{2\alpha p_R} \right) \right] \quad (24)$$

$$C_{0L} \equiv -\rho_R \Delta p \left[c_{in}^2 - \frac{1}{2} \left(\frac{2\alpha p_R - \Delta p}{\rho_R} \right) \right]^2, \quad (25)$$

where the velocity c_{in} is defined as

$$c_{in}^2 \equiv \frac{B_{in}^2}{\mu_0 \rho_{in}} + \alpha \frac{p_{in}}{\rho_{in}}, \quad (26)$$

and we define the pressure difference Δp as

$$\Delta p \equiv p_R - p_L. \quad (27)$$

[23] Equation (21) was derived assuming that the scaling factors given in equations (18)–(20) are unity. If this is not the case, then if ξ is equal to the right hand side divided by the left hand side of equation (18), and ζ is equal to the right hand side divided by the left hand side of equation (20), then the transformation $c_{in}^2 \rightarrow (\zeta/\xi)c_{in}^2$ will algebraically account for scaling factors that are not unity in equations (18) and (20) for equation (21).

[24] Equation (21) simplifies for some special cases. When $\rho_L = \rho_R \equiv \rho_{out}$, the coefficient C_{6L} vanishes, leaving a qua-

dratic equation in V_L^2 . In the incompressible limit with $\rho_{in} = \rho_L = \rho_R \equiv \rho$ and $\alpha = 1$, the solution becomes

$$V_{L,R}^2 \sim \sqrt{4 \left(c_{in}^2 - \frac{\bar{p}}{\rho} \right)^2 + \left(\frac{\Delta p}{2\rho} \right)^2} \pm \frac{\Delta p}{2\rho}, \quad (28)$$

where the plus and minus signs refer to V_L and V_R , respectively, and we define the average downstream pressure \bar{p} as

$$\bar{p} \equiv \frac{p_L + p_R}{2}. \quad (29)$$

Equation (28) gives the expected result that the outflow speed is slower on the side with higher downstream pressure.

[25] Next, consider the special case with $p_L = p_R = p_{out}$, but where the downstream densities can be different. In this case, C_{0L} vanishes, again leaving a quadratic equation. The solution is

$$V_{L,R}^2 \sim c_{in}^2 \sqrt{\frac{\rho_{R,L}}{\rho_{L,R}}} - \alpha \frac{p_{out}}{\rho_{L,R}}, \quad (30)$$

where we ignore factors of order unity. This equation shows that the outflow speed is higher on the low density side. The scalings presented in equations (28) and (30) both reduce to the scaling in equation (16) in the symmetric limit as they should.

[26] Equations (21), (28), and (30) are derived solely from the scaling relations for conservation of mass, energy, and momentum without explicitly assuming a dissipation mechanism [see also *Cassak and Shay, 2007*]. By using equations (13) and (18) (and consequently assuming resistive dissipation inside the current sheet), the inflow speed can be written as

$$\frac{V_{in}}{V_A} \sim \sqrt{\frac{V_L + V_R}{2V_A S}}. \quad (31)$$

Using equations (11) and (31), the reconnection rate is

$$E_y \sim B_{in} \sqrt{\frac{\eta(V_L + V_R)}{2\mu_0 L}}. \quad (32)$$

[27] Solutions of equation (28) for V_L as a function of $p_L - p_{in}$ and $p_R - p_{in}$ in units of the upstream magnetic pressure are presented in Figure 2 for the incompressible limit. The value for V_R can be found by switching the values for $p_L - p_{in}$ and $p_R - p_{in}$. We see that the outflow velocity from one end does not depend strongly on the downstream pressure from the opposite end. In fact, reconnection events (e.g., in the solar atmosphere) do not require bidirectional outflow jets traveling at the Alfvén speed. Rather, in the presence of asymmetric downstream pressure, there can be one Alfvénic jet and one sub-Alfvénic jet [see also *Roussev et al., 2001; Ding et al., 2010*]. As shown by the widely spaced contours in Figure 3, the normalized reconnection rate $S^{1/2} V_{in}/V_A = \sqrt{(V_L + V_R)/2V_A}$ is only weakly dependent on the differ-

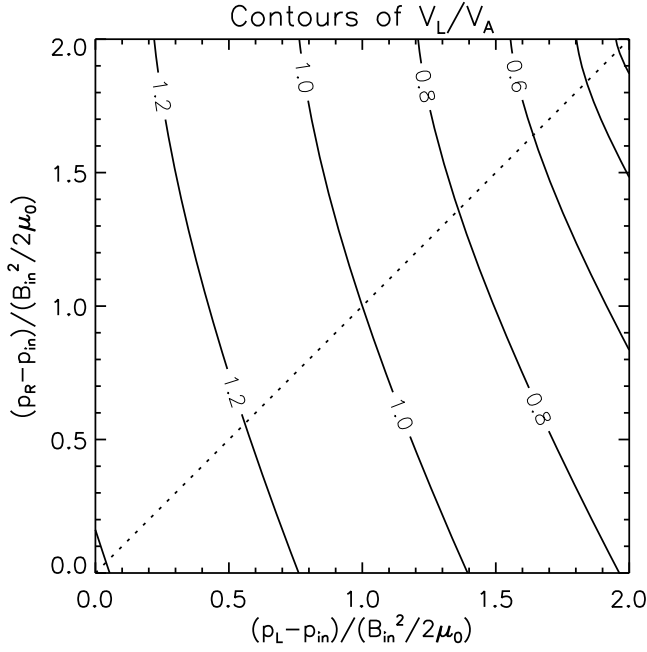


Figure 2. Contours of the outflow velocity from the left side of the current sheet, V_L/V_A , calculated from equation (28) as a function of $p_L - p_{in}$ and $p_R - p_{in}$ for the incompressible case. Contours are separated by 0.2. Figures 2–4 assume that the scaling factors for equations (18)–(20) are unity.

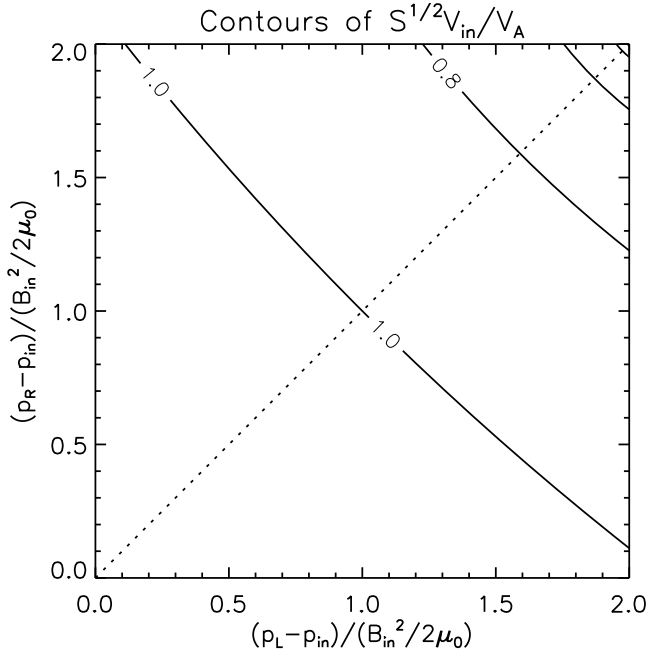


Figure 3. Contours of the normalized reconnection rate, given by $S^{1/2}V_{in}/V_A = \sqrt{(V_L + V_R)/2V_A}$, as a function of $p_L - p_{in}$ and $p_R - p_{in}$ and calculated using equation (28) to find V_L and V_R for the incompressible case. Contours are separated by 0.2.

ence in downstream pressures. This conclusion is consistent with the simulations of X-line retreat reported by *Oka et al.* [2008], in which the reconnection rate is not greatly affected when outflow from one reconnection jet is impeded by the presence of an obstacle while the other outflow jet has no such obstruction.

[28] Figure 4 shows solutions for the incompressible case as a function of $p_L - p_{in}$ for fixed $p_R - p_{in} = B_{in}^2/2\mu_0$. The outflow velocities, calculated using equation (28) and shown in Figures 4a and 4b, illustrate the weak dependence that downstream pressure from one side of the current sheet has on the outflow velocity from the other side of the current sheet. Figures 4c and 4d consider the limiting case where L is prescribed by external influences on geometry and V_{in} varies as a function of p_L and p_R . The normalized reconnection rate, seen in Figure 4c, changes modestly despite the

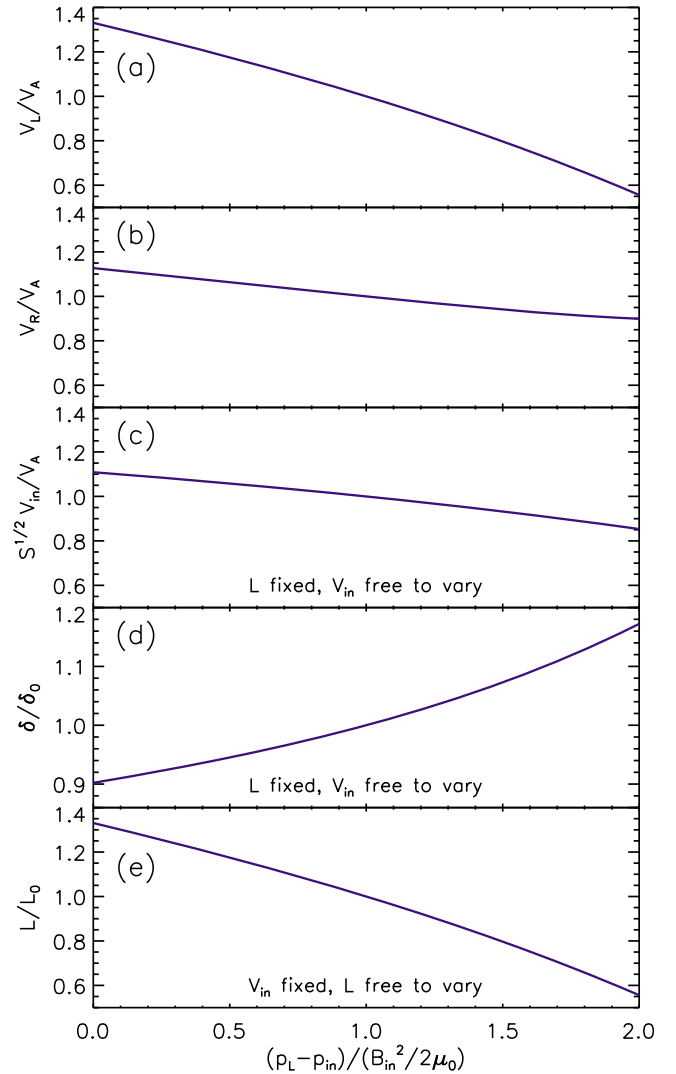


Figure 4. A solution slice along $p_R - p_{in} = B_{in}^2/2\mu_0$ for different values of $p_L - p_{in}$ for the incompressible case. Shown are (a) V_L/V_A , (b) V_R/V_A , (c) $S^{1/2}V_{in}/V_A = \sqrt{(V_L + V_R)/2V_A}$, (d) δ/δ_0 , and (e) L/L_0 . Figures 4c and 4d describe the limiting case where L is prescribed by the global geometry and that V_{in} is free to vary, whereas Figure 4e assumes that V_{in} is prescribed externally and that L is free to vary.

large change in p_L . Defining $\delta_0 \equiv \sqrt{\eta L / \mu_0 V_A}$, we see that $\delta / \delta_0 = \sqrt{2V_A / (V_L + V_R)}$ increases with p_L . The increased current sheet thickness slows the reconnection rate slightly by equation (13). Figure 4e considers a different limiting case for which V_{in} is prescribed due to external driving of reconnection and L varies as a function of p_L and p_R to maintain the same reconnection rate. For this case, δ is given by equation (13) and is independent of downstream pressure. Defining $L_0 \equiv \eta V_A / \mu_0 V_{in}^2$, the normalized length is given by $L/L_0 = (V_L + V_R)/2V_A$. Figure 4e shows that greater downstream pressure reduces the length of the current sheet for this case, and hence the throughput of mass, in response to greater downstream pressure.

3.3. Internal Structure

[29] Now that the global quantities associated with a current sheet with asymmetric downstream pressure can be found, we turn our attention to the internal structure of the current sheet. It has been observed in simulations that asymmetry in the outflow direction can lead to a separation of the X-line and flow stagnation point [e.g., *Laitinen et al.*, 2005; *Laitinen*, 2007]. Therefore, we divide the current sheet into three regions of lengths L_L , L_M , and L_R , with boundaries at the flow stagnation point and magnetic field null as indicated in Figure 1. The length L_M is the distance between the magnetic field null and the flow stagnation point, which we will see need not be zero. The full length of the current sheet, $2L$, is given by

$$2L = L_L + L_M + L_R. \quad (33)$$

[30] For the rest of this section we assume for simplicity that the upstream fields are describable by approximately uniform values and that the current sheet thickness is approximately constant throughout the diffusion region. While in general there will be some variation of these quantities along the outflow direction, this assumption allows us to perform a straightforward analysis of the internal structure of a simple asymmetric current sheet.

[31] As in the model by *Cassak and Shay* [2007], the position of the flow stagnation point is set by conservation of mass. Evaluating equation (7) for the three sections of the current sheet presented in Figure 1 yields the conservation of mass relations

$$\rho_{in} V_{in} L_L \sim \rho_L V_L \delta, \quad (34)$$

$$\rho_{in} V_{in} L_M \sim \rho_n V_n \delta, \quad (35)$$

$$\rho_{in} V_{in} (L_M + L_R) \sim \rho_R V_R \delta. \quad (36)$$

where ρ_n is the density and V_n is the outflow component of velocity at the magnetic field null. The location of the flow stagnation point can be derived from equations (33), (34), and (36), and is given by the relations

$$L_L \sim 2L \left(\frac{\rho_L V_L}{\rho_L V_L + \rho_R V_R} \right), \quad (37)$$

$$L_M + L_R \sim 2L \left(\frac{\rho_R V_R}{\rho_L V_L + \rho_R V_R} \right). \quad (38)$$

[32] Evaluating the conservation of energy surface integral given in equation (9) in a similar way yields

$$V_{in} L_L \left[\alpha p_{in} + \frac{B_{in}^2}{\mu_0} \right] + V_{in} \delta \left(\frac{B_{in} B_s}{\mu_0} \right) \sim V_L \delta \left[\alpha p_L + \frac{\rho_L V_L^2}{2} \right], \quad (39)$$

$$V_{in} L_M \left[\alpha p_{in} + \frac{B_{in}^2}{\mu_0} \right] \sim V_{in} \delta \left(\frac{B_{in} B_s}{\mu_0} \right) + V_n \delta \left[\alpha p_n + \frac{\rho_n V_n^2}{2} \right], \quad (40)$$

$$V_{in} L_R \left[\alpha p_{in} + \frac{B_{in}^2}{\mu_0} \right] + V_n \delta \left[\alpha p_n + \frac{\rho_n V_n^2}{2} \right] \sim V_R \delta \left[\alpha p_R + \frac{\rho_R V_R^2}{2} \right], \quad (41)$$

where B_s is the vertical magnetic field strength at the flow stagnation point. When the magnetic field null and flow stagnation point are separated, there is a Poynting flux across the flow stagnation point and a kinetic energy flux across the magnetic field null.

[33] While, in principle, equations (39)–(41) can be used with additional relations to solve for L_L , L_M , and L_R , we proceed using an alternate argument to find the separation between the magnetic field null and flow stagnation point. In a steady state, the outflow component of the momentum equation along $z = 0$ reduces to

$$\rho V_x \frac{\partial V_x}{\partial x} = \frac{B_z}{\mu_0} \frac{\partial B_x}{\partial z} - \frac{\partial p}{\partial x}, \quad (42)$$

where we assume that the magnetic pressure inside the current sheet is small compared to magnetic tension. At the flow stagnation point, the magnetic tension force must cancel the pressure gradient force in a steady-state system. Moreover, the magnetic field null is collocated with the flow stagnation point in a steady state only when there is no pressure gradient at the magnetic field null.

[34] To quantify this, define x_n as the position of the magnetic field null and x_s as the position of the flow stagnation point. By definition, x_s is given by $V_x(x_s) \equiv 0$. Evaluating equation (42) at the flow stagnation point using equation (12) gives

$$\frac{B_s(x_s)}{\mu_0} \frac{B_m}{\delta} \sim \frac{\partial p}{\partial x} \Big|_{x=x_s}. \quad (43)$$

Using that $B_z(x_n) \equiv 0$, a Taylor expansion to first order yields

$$B_z(x_s) \simeq (x_s - x_n) \frac{\partial B_z}{\partial x} \Big|_{x=x_n}. \quad (44)$$

Hence, we can approximate the distance between the flow stagnation point and the magnetic field null for a steady state,

$$L_M = x_n - x_s \sim \left(\frac{\mu_0 \delta}{B_{in}} \right) \left(\frac{-\partial p / \partial x|_{x=x_s}}{\partial B_z / \partial x|_{x=x_n}} \right). \quad (45)$$

4. Comparison to Simulations

[35] In this section, we test the scaling relations and results derived in section 3 using resistive MHD simulations for the configuration of MRX, but with the geometry straightened from cylindrical to linear. Asymmetry in the outflow direction develops for the push mode of operation [see *Yamada et al.*, 1997, Figure 5] when one downstream wall is closer to the current sheet than the other downstream wall. The driving process in these simulations constrains the position of the reconnection layer and thus limits time-dependent motion of the current sheet. Except as otherwise noted, the numerical method and simulation setup are as described by *Murphy and Sovinec* [2008].

4.1. Numerical Method and Problem Setup

[36] The NIMROD code (Non-Ideal Magnetohydrodynamics with Rotation, Open Discussion) [*Sovinec et al.*, 2004] has been successfully used to model reconnection in a variety of geometries [e.g., *Hooper et al.*, 2005; *Murphy and Sovinec*, 2008; *Zhu et al.*, 2009]. NIMROD uses a finite element expansion in the poloidal plane and, in three-dimensional simulations, a Fourier representation for the out-of-plane direction. The system of equations solved by NIMROD for the two-dimensional simulations reported in this section are

$$\frac{\partial \mathbf{B}}{\partial t} = -\nabla \times (\eta \mathbf{J} - \mathbf{V} \times \mathbf{B}) + \kappa_{divb} \nabla(\nabla \cdot \mathbf{B}), \quad (46)$$

$$\mu_0 \mathbf{J} = \nabla \times \mathbf{B}, \quad (47)$$

$$\rho \left(\frac{\partial \mathbf{V}}{\partial t} + \mathbf{V} \cdot \nabla \mathbf{V} \right) = \mathbf{J} \times \mathbf{B} - \nabla p + \nabla \cdot \rho \nu \nabla \mathbf{V}, \quad (48)$$

$$\frac{\partial n}{\partial t} + \nabla \cdot (n \mathbf{V}) = \nabla \cdot D \nabla n, \quad (49)$$

$$\frac{n}{\gamma - 1} \left(\frac{\partial T}{\partial t} + \mathbf{V} \cdot \nabla T \right) = -\frac{p}{2} \nabla \cdot \mathbf{V} - \nabla \cdot \mathbf{q} + Q, \quad (50)$$

where the heat source term $Q = \eta \mathbf{J}^2 + \nu \rho \nabla \mathbf{V}^T \cdot \nabla \mathbf{V}$ includes Ohmic and viscous heating, isotropic thermal conduction $\mathbf{q} = -n \chi \nabla T$ is used, ν is the kinematic viscosity, χ is the thermal diffusivity, and D is an artificial number density diffusivity.

[37] The last term on the right side of equation (46) is used to control numerical divergence error. This approach is effective and accurate with high-order finite elements [*Sovinec et al.*, 2004], and numerical convergence has been checked in the simulations reported here. The ratio of specific heats is given by $\gamma = 5/3$, which corresponds to $\alpha \equiv \gamma/(\gamma - 1) = 2.5$. The resistivity is given by $\eta/\mu_0 = 20 \text{ m}^2 \text{ s}^{-1}$, which corresponds to a Lundquist number of $S \sim 100$ using the half-length of the current sheet and the immediately upstream magnetic field strength and density. The magnetic Prandtl number is given by $\text{Pm} \equiv \nu/(\eta/\mu_0) = 0.25$, with $\nu = D = \chi = 5 \text{ m}^2 \text{ s}^{-1}$. Reconnection is driven by applying an electric field on the surfaces of two flux cores which have a minor radius of 9.4 cm and are located at $(x, z) = (0 \text{ cm}, \pm 27 \text{ cm})$

using the coordinate system established in section 3. In linear geometry, the flux cores are infinite cylinders. The upper and lower boundaries are at $z = \pm 62 \text{ cm}$. For one run, the downstream boundaries are at $x = -22.5 \text{ cm}$ and $x = 32.5 \text{ cm}$ (case A). For the other run, the downstream boundaries are at $x = -17.5 \text{ cm}$ and $x = 32.5 \text{ cm}$ (case B).

4.2. Simulation Results

[38] Next, we present results from these simulations and compare them to the model presented in this paper. A cut along $z = 0$ from case B at $13.3 \mu\text{s}$ is shown in Figure 5. At this time, the flow stagnation point is at $x = 1.42 \text{ cm}$ and the magnetic field null is at $x = 1.82 \text{ cm}$, indicating a short separation between the two points. Over most of the simulated time the flow stagnation point is located closer to the side with the impeded outflow than the magnetic field null in qualitative agreement with equation (45). The resistive electric field dominates in the central regions of the current sheet whereas the convective electric field dominates as the outflow approaches its peak value. Magnetic pressure is not important within the current sheet.

[39] To perform quantitative comparisons with theory, the relevant quantities must be extracted from the numerical results. The full length $2L$ of the current sheet is taken to be the distance along $z = 0$ between the two locations where the out-of-plane current density drops to a fraction f of its peak value, where f is either $1/e$ or $1/e^2$. The thickness of the current sheet, δ , is taken to be the distance in the z direction between the location where the out-of-plane current density peaks and where it falls off to f of its peak value. The values for the upstream fields are extracted from the simulation at $z = \pm \delta$ above and below where the current density peaks. This method slightly but systematically underestimates the upstream magnetic field strength. The values for the downstream fields are taken at $z = 0$ where the out-of-plane current density falls to f of its peak value.

[40] Comparisons between simulation and our scaling relations are shown in Figure 6, using both of the aforementioned values of f for both case A and case B. Figure 6a compares the left and right hand sides of equation (18) which approximates conservation of mass, Figure 6b compares the left and right hand sides of equation (19) regarding momentum balance, and Figure 6c compares the left and right hand sides of equation (20) which approximates conservation of energy. Verification of these scaling relations requires that the data reasonably fit a straight line through the origin. In Figures 6a–6c, we see that the left and right hand sides of each of the equations approximately fit straight lines through the origin with slopes close to unity. In Figures 6a and 6c, the slope is slightly greater than unity (~ 1.15 – 1.2).

[41] Comparisons between the outflow velocities extracted from simulation and calculated as roots of equation (21) are shown in Figures 7a and 7b. Because the positions (and even existence within the set of real numbers) of roots of high order polynomials can be sensitive to small changes in the coefficients [e.g., *Wilkinson*, 1959], modest differences between the left and right hand sides of equations (18), (19), or (20) sometimes lead to large errors in the solution for V_L and V_R or the relevant root becoming complex. Because of this property common among high order polynomials, not all of the instances considered have real roots and there is

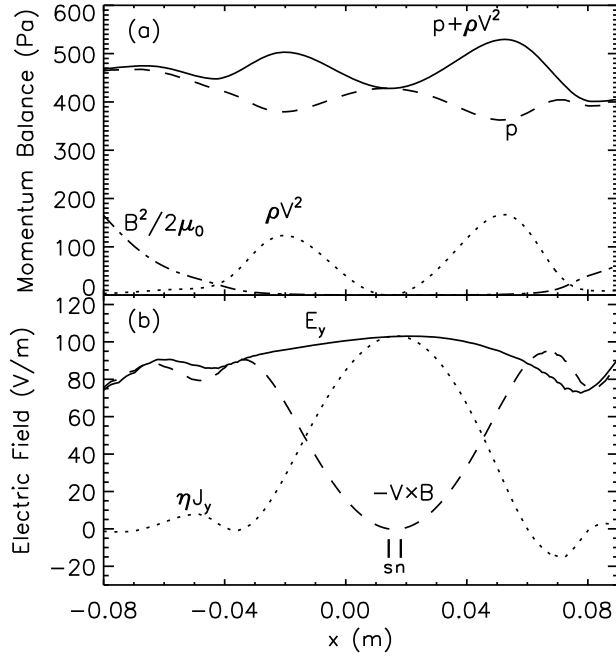


Figure 5. A slice in the outflow direction along $z = 0$ of terms from (a) momentum balance and (b) electric field balance for case B at $t = 13.3 \mu\text{s}$. Vertical bars represent the positions of the flow stagnation point (marked ‘s’) and the magnetic field null (marked ‘n’).

increased scatter in Figures 7a and 7b beyond what is seen in Figure 6. Despite this, the simulation results show reasonable agreement for instances where the roots of the polynomials are not greatly impacted by scaling factors that are not unity in equations (18), (19), and (20). The expression for the reconnection electric field strength given by equation (32) is compared against simulation in Figure 7c, showing good agreement despite a small underprediction of $\sim 10\text{--}20\%$. The positions of the flow stagnation point given by equations (37)

and (38) are tested against the simulation results in Figure 8. Despite some outliers, most of the data points show a good correspondence between the model predictions and the simulation results. The scatter is primarily due to time-dependent effects and the non-uniformity of the upstream fields. However, the presence of a local pressure maximum near the flow stagnation point and magnetic field null complicates the determination of L_M for most cases because the pressure gradient varies significantly in this region; consequently, equation (45) does not reliably predict the separation between the flow stagnation point and magnetic field null for these cases.

[42] As a final check for the assumptions of this model, the surface integrals in equations (7)–(9) are calculated along the current sheet boundaries using the finite element basis functions to interpolate the data. Evaluating the conservation of mass integral in equation (7) shows that the mass influx is within $\sim 10\text{--}25\%$ of the mass efflux, indicating modest time-dependence. Evaluating the conservation of energy integral given in equation (9) shows that the contribution from the term proportional to plasma pressure is the largest for both the upstream and downstream boundaries. During the early stages of reconnection the Poynting flux out of the layer is comparable to the kinetic energy efflux, but as reconnection continues to develop the Poynting flux becomes small ($\leq 15\%$) compared to the kinetic energy efflux. Evaluating the outflow component of the conservation of momentum integral given in equation (8) again shows that the plasma pressure term is dominant. Early in time, the downstream magnetic pressure due to the vertical magnetic field is comparable to the momentum flux out of the layer but becomes small in comparison as reconnection develops and the outflow velocities increase with time. Magnetic tension forces associated with the upstream boundaries are of the same order as the momentum flux exiting each side of the layer but are smaller than the contribution from terms proportional to pressure. The integrated tension forces towards each downstream region are symmetric to within $\sim 5\text{--}30\%$ for case A, but for case B, the

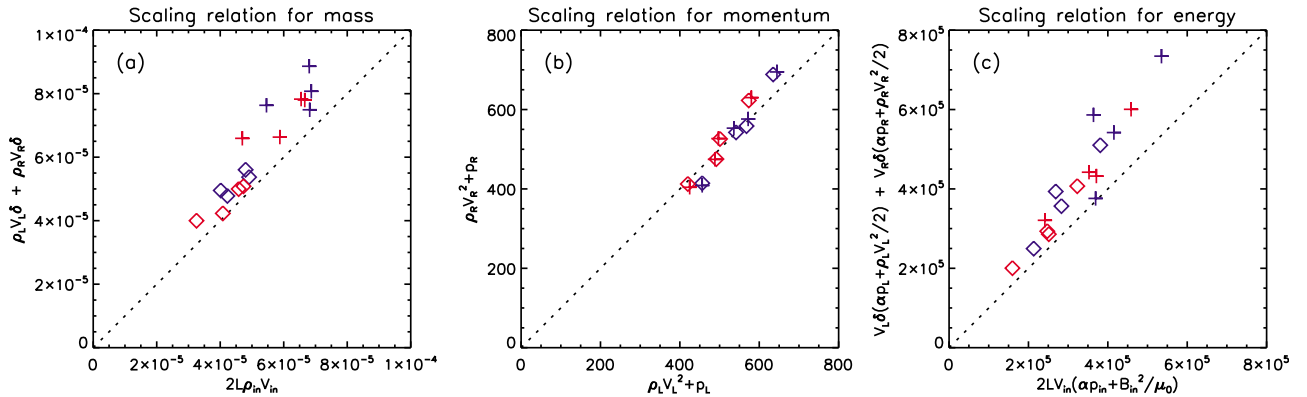


Figure 6. Comparisons between the scaling relationships derived in section 3 and the simulation results. Shown in SI units are the left and right hand sides of equations (18)–(20) representing scaling relations for (a) mass, (b) momentum, and (c) energy. The data points representing cases A and B are plotted in blue and red, respectively, for $f = e^{-1}$ (diamonds) and $f = e^{-2}$ (plus signs). The data were extracted at $9.1 \mu\text{s}$, $11.2 \mu\text{s}$, $13.3 \mu\text{s}$, and $15.4 \mu\text{s}$. The dotted line represents a one-to-one correspondence between the left and right hand sides of each scaling relation.

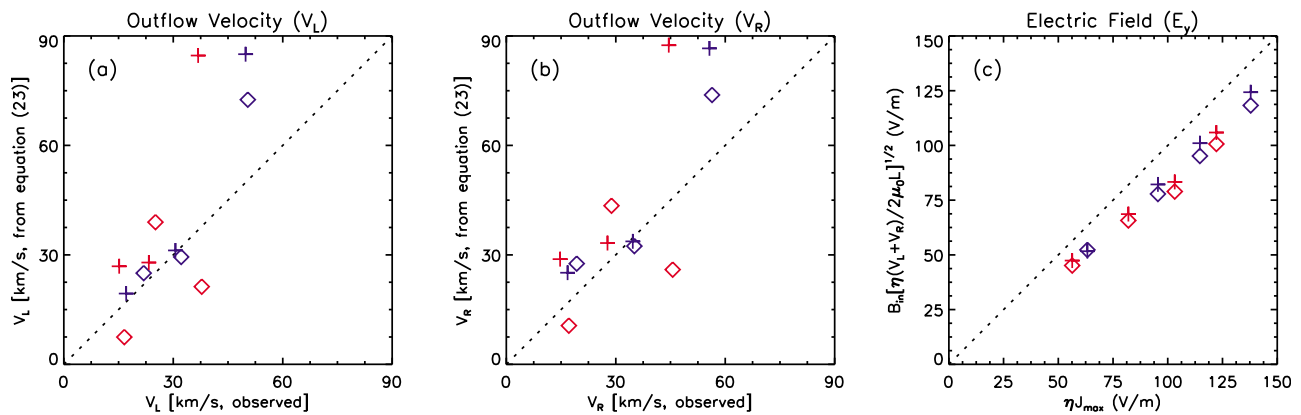


Figure 7. Comparisons between model predictions and simulation results. Shown are (a) the outflow velocity V_L compared against equation (21), (b) the outflow velocity V_R compared against equation (21), and (c) the electric field E_y compared against equation (32). The symbol usage is described in Figure 6.

total tension force directed towards the obstructing wall is ~ 2 – 3 times larger than the total tension force directed towards positive x . Thus the full evaluation of these surface integrals shows that equations (18) and (20) representing conservation of mass and energy can be used to successfully describe the scaling of steady magnetic reconnection with asymmetry in the outflow direction. However, for modest aspect ratio current sheets such as those associated with the Earth’s magnetotail or spheromak merging, contributions to tension along the boundary can be important for momentum balance in the outflow direction and need to be considered further in future work.

5. Summary and Conclusions

[43] Magnetic reconnection with asymmetry in the outflow direction occurs in many systems in nature and in the laboratory, including planetary magnetotails, coronal mass ejections, flux cancellation events, laboratory reconnection experiments, astrophysical disks, and magnetized turbulence. In this paper, we perform a control volume analysis to describe long and thin current sheets with asymmetric downstream pressure and test these scalings using resistive MHD simulations of driven reconnection.

[44] In section 3, we derive a set of scaling relationships which describe steady-state magnetic reconnection in a current sheet with asymmetry in the outflow direction without explicitly specifying the dissipation mechanism. We derive expressions for the outflow velocity for both the compressible and incompressible cases that do not directly depend on the dissipation mechanism. When resistive dissipation is assumed, we present an expression for the reconnection rate that depends on the outflow velocities from both sides of the current sheet. Together, these relations show how the outflow velocities and reconnection rate depend on a combination of upstream and downstream parameters. In the presence of asymmetric downstream pressure, it is possible to have one Alfvénic jet and one sub-Alfvénic jet rather than two bidirectional Alfvénic jets. The reconnection rate is greatly reduced only when outflow from both sides of the current sheet is blocked. This helps explain

results by *Oka et al.* [2008], who found that the presence of an obstacle on one downstream side of the current sheet does not greatly impact the reconnection rate, and by *Nakamura et al.* [2010], who found that initial X-lines near the edges of a region of multiple X-lines tend to win out over X-lines in the central part of that region.

[45] In a steady state, the magnetic field null and flow stagnation point overlap only in the absence of pressure gradient forces at the magnetic field null. When there is a pressure gradient, the magnetic field null is located on the side of the flow stagnation point which allows magnetic tension to counter the non-electromagnetic forces at the flow stagnation point. The position of the flow stagnation point can be estimated using conservation of mass when the upstream density and inflow velocity are approximately

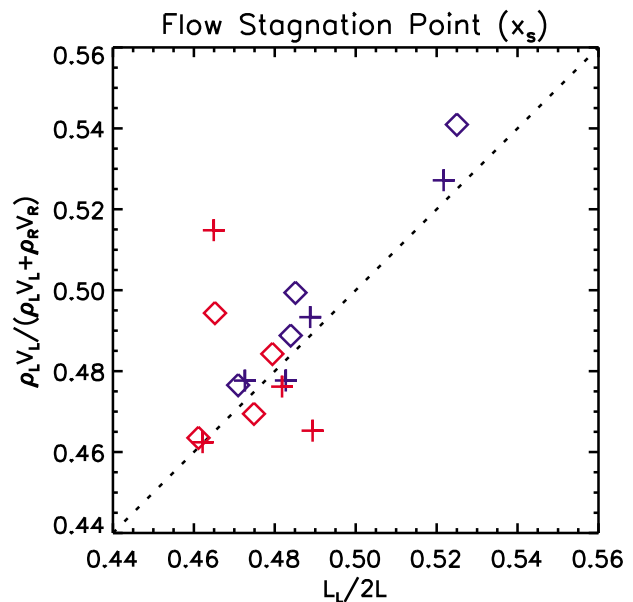


Figure 8. The position of the flow stagnation point observed in simulation compared against the relation given by equation (37). The symbol usage is explained in Figure 6.

uniform. The position of the magnetic field null relative to the flow stagnation point can be estimated using a Taylor expansion around the flow stagnation point.

[46] To test the scaling relations derived in this paper, we perform two-dimensional resistive MHD simulations of driven reconnection using the setup of MRX in linear geometry. Asymmetry in the outflow direction develops because one downstream wall is closer to the current sheet than the other downstream wall. The driving mechanism of MRX constrains the current sheet position between the flux cores and limits current sheet motion. Data extracted from this test show good correspondence with the scaling relations approximating conservation of mass, momentum, and energy. The solution of equation (21) for outflow velocities shows reasonable agreement but increased scatter since the roots of high order polynomials can be sensitive to small errors in the coefficients. The reconnection electric field strength and the flow stagnation point position are well predicted by equations (32) and (37). The position of the magnetic field null is not well predicted by equation (45) due to the presence of a local pressure maximum near these two points. Exact evaluation of the integrals show that most of the assumptions of the model are reasonably met but that there is a non-negligible contribution due to tension along the boundary of the current sheet.

[47] There are many opportunities in both nature and the laboratory to investigate the impact of asymmetry on the reconnection process. The pull mode of operation in MRX is well-suited to investigate reconnection with asymmetry in the inflow direction due to cylindrical geometry effects [Murphy and Sovinec, 2008]. However, effects related to downstream pressure may need to be incorporated into the scaling relations of Cassak and Shay [2007]. SSX, TS-3/4, and the push mode of operation in MRX can be used to study the impact of asymmetry in the outflow direction [e.g., Inomoto et al., 2006]. Observing reconnection with asymmetry in the outflow direction in the magnetosphere requires multiple satellites located both earthward and tailward of the reconnection site at approximately the same time. While statistical approaches are possible [e.g., Petrukovich et al., 2009], observations of a single event are not common (for a possible example, see Laitinen et al. [2007]). Remote sensing observations of solar reconnection phenomena such as flux cancellation events, chromospheric jets, solar flares, and coronal mass ejections can also be used to provide information on the effects of asymmetry in the outflow direction.

[48] The model developed in this paper assumes steady-state two-dimensional antiparallel reconnection in a current sheet with $\delta \ll L$. Refinements or alternatives to this analysis would benefit from the inclusion of time-dependent effects such as current sheet motion and plasmoid formation. Of particular interest are what determines the rate of X-line retreat as seen in simulations by Oka et al. [2008] and how the current sheet structure and dynamics are changed due to current sheet motion. Three-dimensional effects have the potential to enhance the ability of plasma to exit the current sheet [e.g., Lazarian and Vishniac, 1999; Sullivan and Rogers, 2008; Shimizu et al., 2009]. Future analyses should consider the uneven contribution of magnetic tension for modest aspect ratio current sheets. This would allow the effect noted by Galsgaard et al. [2000], Galsgaard and

Roussev [2002], and Murphy and Sovinec [2008], in which asymmetric outflow develops because the X-point is displaced towards one end of the current sheet, to be quantified.

[49] **Acknowledgments.** The authors thank Ellen Zweibel, Jennifer Stone, Michiaki Inomoto, John Raymond, Ping Zhu, Yi-Min Huang, Michael Shay, Clare Parnell, Dmitri Uzdensky, Mitsuo Oka, Joseph Cassinelli, Richard Townsend, K. Tabetha Hole, John Everett, Seth Dorfman, and Samuel Friedman for useful discussions. N. A. M. and C. R. S. acknowledge support from NSF grant PHY-0821899 through the Center for Magnetic Self-Organization in Laboratory and Astrophysical Plasmas. N. A. M. acknowledges additional support from NASA grant NNX09AB17G to the Smithsonian Astrophysical Observatory. P. A. C. acknowledges support from NSF grant PHY-0902479. This research has benefited from use of NASA's Astrophysics Data System Bibliographic Services.

[50] Philippa Browning thanks Terry Forbes and Clare Parnell for their assistance in evaluating this paper.

References

- Aurass, H., B. Vršnak, and G. Mann (2002), Shock-excited radio burst from reconnection outflow jet?, *Astron. Astrophys.*, *384*, 273–281, doi:10.1051/0004-6361:20011735.
- Aurass, H., F. Landini, and G. Poletto (2009), Coronal current sheet signatures during the 17 May 2002 CME-flare, *Astron. Astrophys.*, *506*, 901–911, doi:10.1051/0004-6361/200912229.
- Bemporad, A. (2008), Spectroscopic detection of turbulence in post-CME current sheets, *Astrophys. J.*, *689*, 572–584, doi:10.1086/592377.
- Bemporad, A., G. Poletto, S. T. Suess, Y. Ko, N. A. Schwadron, H. A. Elliott, and J. C. Raymond (2006), Current sheet evolution in the aftermath of a CME event, *Astrophys. J.*, *638*, 1110–1128, doi:10.1086/497529.
- Birn, J., and M. Hesse (2009), Reconnection in substorms and solar flares: Analogies and differences, *Ann. Geophys.*, *27*, 1067–1078.
- Birn, J., M. Hesse, and K. Schindler (1996), MHD simulations of magnetotail dynamics, *J. Geophys. Res.*, *101*, 12,939–12,954, doi:10.1029/96JA00611.
- Birn, J., J. E. Borovsky, and M. Hesse (2008), Properties of asymmetric magnetic reconnection, *Phys. Plasmas*, *15*(3), 032101, doi:10.1063/1.2888491.
- Borovsky, J. E., and M. Hesse (2007), The reconnection of magnetic fields between plasmas with different densities: Scaling relations, *Phys. Plasmas*, *14*(10), 102309, doi:10.1063/1.2772619.
- Borovsky, J. E., M. Hesse, J. Birn, and M. M. Kuznetsova (2008), What determines the reconnection rate at the dayside magnetosphere?, *J. Geophys. Res.*, *113*, A07210, doi:10.1029/2007JA012645.
- Brown, M. R., C. D. Cothran, and J. Fung (2006), Two fluid effects on three-dimensional reconnection in the Swarthmore Spheromak Experiment with comparisons to space data, *Phys. Plasmas*, *13*(5), 056503, doi:10.1063/1.2180729.
- Cassak, P. A., and M. A. Shay (2007), Scaling of asymmetric magnetic reconnection: General theory and collisional simulations, *Phys. Plasmas*, *14*(10), 102114, doi:10.1063/1.2795630.
- Cassak, P. A., and M. A. Shay (2008), Scaling of asymmetric Hall magnetic reconnection, *Geophys. Res. Lett.*, *35*, L19102, doi:10.1029/2008GL035268.
- Cassak, P. A., and M. A. Shay (2009), Structure of the dissipation region in fluid simulations of asymmetric magnetic reconnection, *Phys. Plasmas*, *16*, 055704, doi:10.1063/1.3086867.
- Cassinelli, J. P., J. C. Brown, M. Maheswaran, N. A. Miller, and D. C. Telfer (2002), A magnetically torqued disk model for Be stars, *Astrophys. J.*, *578*, 951–966, doi:10.1086/342654.
- Chae, J., Y.-J. Moon, and S.-Y. Park (2003), Observational tests of chromospheric magnetic reconnection, *J. Korean Astron. Soc.*, *36*, S13–S20.
- Chen, L.-J., et al. (2009), Multispacecraft observations of the electron current sheet, neighboring magnetic islands, and electron acceleration during magnetotail reconnection, *Phys. Plasmas*, *16*(5), 056501, doi:10.1063/1.3112744.
- Chen, P. F., K. Shibata, D. H. Brooks, and H. Isobe (2004), A reexamination of the evidence for reconnection inflow, *Astrophys. J. Lett.*, *602*, L61–L64, doi:10.1086/382479.
- Ciaravella, A., and J. C. Raymond (2008), The current sheet associated with the 2003 November 4 coronal mass ejection: Density, temperature, thickness, and line width, *Astrophys. J.*, *686*, 1372–1382, doi:10.1086/590655.

- Ciaravella, A., J. C. Raymond, J. Li, P. Reiser, L. D. Gardner, Y. Ko, and S. Fineschi (2002), Elemental abundances and post-coronal mass ejection current sheet in a very hot active region, *Astrophys. J.*, *575*, 1116–1130, doi:10.1086/341473.
- Cothran, C. D., A. Falk, A. Fefferman, M. Landreman, M. R. Brown, and M. J. Schaffer (2003), Spheromak merging and field reversed configuration formation at the Swarthmore Spheromak Experiment, *Phys. Plasmas*, *10*, 1748–1754, doi:10.1063/1.1564084.
- Ding, J. Y., M. S. Madjarska, J. G. Doyle, and Q. M. Lu (2010), Chromospheric magnetic reconnection caused by photospheric flux emergence: Implications for jet-like events formation, *Astron. Astrophys.*, *510*, A111, doi:10.1051/0004-6361/200913101.
- Drake, J. F., M. Swisdak, H. Che, and M. A. Shay (2006), Electron acceleration from contracting magnetic islands during reconnection, *Nature*, *443*, 553–556, doi:10.1038/nature05116.
- Eriksson, S., et al. (2009), Asymmetric shear flow effects on magnetic field configuration within oppositely directed solar wind reconnection exhausts, *J. Geophys. Res.*, *114*, A07103, doi:10.1029/2008JA013990.
- Galsgaard, K., and I. Roussev (2002), Magnetic reconnection in 2D stratified atmospheres. I. Dynamical consequences, *Astron. Astrophys.*, *383*, 685–696, doi:10.1051/0004-6361:20011733.
- Galsgaard, K., C. E. Parnell, and J. Blaizot (2000), Elementary heating events—Magnetic interactions between two flux sources, *Astron. Astrophys.*, *362*, 395–405.
- Goedbloed, J. P., and S. Poedts (2004), *Principles of Magnetohydrodynamics*, Cambridge Univ. Press, Cambridge, U. K.
- Gontikakis, C., V. Archontis, and K. Tsinganos (2009), Observations and 3D MHD simulations of a solar active region jet, *Astron. Astrophys.*, *506*, L45–L48, doi:10.1051/0004-6361/200913026.
- Hesse, M., and K. Schindler (2001), The onset of magnetic reconnection in the magnetotail, *Earth Planets Space*, *53*, 645–653.
- Hesse, M., J. Birn, D. N. Baker, and J. A. Slavin (1996), MHD simulations of the transition of magnetic reconnection from closed to open field lines, *J. Geophys. Res.*, *101*, 10,805–10,816, doi:10.1029/95JA02857.
- Hooper, E. B., T. A. Kopriva, B. I. Cohen, D. N. Hill, H. S. McLean, R. D. Wood, S. Woodruff, and C. R. Sovinec (2005), Magnetic reconnection during flux conversion in a driven spheromak, *Phys. Plasmas*, *12*(9), 092503, doi:10.1063/1.2040207.
- Innes, D. E., B. Inhester, W. I. Axford, and K. Willhelm (1997), Bidirectional plasma jets produced by magnetic reconnection on the Sun, *Nature*, *386*, 811–813, doi:10.1038/386811a0.
- Inomoto, M., S. P. Gerhardt, M. Yamada, H. Ji, E. Belova, A. Kuritsyn, and Y. Ren (2006), Coupling between global geometry and the local Hall effect leading to reconnection-layer symmetry breaking, *Phys. Rev. Lett.*, *97*(13), 135002, doi:10.1103/PhysRevLett.97.135002.
- Kiehas, S. A., V. S. Semenov, I. V. Kubyshkin, Y. V. Tolstykh, T. Penz, and H. K. Biernat (2007), Effects of a moving X-line in a time-dependent reconnection model, *Ann. Geophys.*, *25*, 293–302.
- Kiehas, S., et al. (2009), First application of a Petschek-type reconnection model with time-varying reconnection rate to THEMIS observations, *J. Geophys. Res.*, *114*, A00C20, doi:10.1029/2008JA013528.
- Ko, Y., J. C. Raymond, J. Lin, G. Lawrence, J. Li, and A. Fludra (2003), Dynamical and physical properties of a post-coronal mass ejection current sheet, *Astrophys. J.*, *594*, 1068–1084, doi:10.1086/376982.
- Kopp, R. A., and G. W. Pneuman (1976), Magnetic reconnection in the corona and the loop prominence phenomenon, *Sol. Phys.*, *50*, 85–98, doi:10.1007/BF00206193.
- Kuznetsova, M. M., M. Hesse, L. Rastätter, A. Taktakishvili, G. Toth, D. L. De Zeeuw, A. Ridley, and T. I. Gombosi (2007), Multiscale modeling of magnetospheric reconnection, *J. Geophys. Res.*, *112*, A10210, doi:10.1029/2007JA012316.
- La Belle-Hamer, A. L., A. Otto, and L. C. Lee (1995), Magnetic reconnection in the presence of sheared flow and density asymmetry: Applications to the Earth's magnetopause, *J. Geophys. Res.*, *100*(A7), 11,875–11,890.
- Laitinen, T. V. (2007), Rekonnetio Maan Magnetosfäärissä, Ph.D. thesis, Finn. Meteorol. Inst., Helsinki.
- Laitinen, T. V., T. I. Pulkkinen, M. Palmroth, P. Janhunen, and H. E. J. Koskinen (2005), The magnetotail reconnection region in a global MHD simulation, *Ann. Geophys.*, *23*, 3753–3764.
- Laitinen, T. V., R. Nakamura, A. Runov, H. Rème, and E. A. Lucek (2007), Global and local disturbances in the magnetotail during reconnection, *Ann. Geophys.*, *25*, 1025–1035.
- Lazarian, A., and E. T. Vishniac (1999), Reconnection in a weakly stochastic field, *Astrophys. J.*, *517*, 700–718, doi:10.1086/307233.
- Lee, L. C., and Z. F. Fu (1986), Multiple X line reconnection: I. A criterion for the transition from a single X line to a multiple X line reconnection, *J. Geophys. Res.*, *91*, 6807–6815, doi:10.1029/JA091iA06p06807.
- Lin, J., and T. G. Forbes (2000), Effects of reconnection on the coronal mass ejection process, *J. Geophys. Res.*, *105*, 2375–2392, doi:10.1029/1999JA900477.
- Lin, J., J. Li, T. G. Forbes, Y. Ko, J. C. Raymond, and A. Vourlidas (2007), Features and properties of coronal mass ejection/flare current sheets, *Astrophys. J. Lett.*, *658*, L123–L126, doi:10.1086/515568.
- Lin, J., S. R. Cranmer, and C. J. Farrugia (2008), Plasmoids in reconnecting current sheets: Solar and terrestrial contexts compared, *J. Geophys. Res.*, *113*, A11107, doi:10.1029/2008JA013409.
- Lin, J., J. Li, Y. Ko, and J. C. Raymond (2009), Investigation of thickness and electrical resistivity of the current sheets in solar eruptions, *Astrophys. J.*, *693*, 1666–1677, doi:10.1088/0004-637X/693/2/1666.
- Lin, Y., X. Y. Wang, M. R. Brown, M. J. Schaffer, and C. D. Cothran (2008), Modeling Swarthmore spheromak reconnection experiment using hybrid code, *Plasma Phys. Controlled Fusion*, *50*(7), 074012, doi:10.1088/0741-3335/50/7/074012.
- Litvinenko, Y. E. (1999), Photospheric magnetic reconnection and canceling magnetic features on the Sun, *Astrophys. J.*, *515*, 435–440, doi:10.1086/307001.
- Litvinenko, Y. E., and J. Chae (2009), Signatures of Sweet-Parker magnetic reconnection in the solar chromosphere, *Astron. Astrophys.*, *495*, 953–957, doi:10.1051/0004-6361:200811034.
- Liu, W., T. E. Berger, A. M. Title, and T. D. Tarbell (2009), An intriguing chromospheric jet observed by Hinode: Fine structure kinematics and evidence of unwinding twists, *Astrophys. J. Lett.*, *707*, L37–L41.
- Lui, A. T. Y., H. E. Spence, and D. P. Stern (1994), Empirical modeling of the quiet time nightside magnetosphere, *J. Geophys. Res.*, *99*, 151–157.
- Martin, S. F., S. H. B. Livi, and J. Wang (1985), The cancellation of magnetic flux. II—In a decaying active region, *Aust. J. Phys.*, *38*, 929–959.
- Mozer, F. S., and P. L. Pritchett (2009), Regions associated with electron physics in asymmetric magnetic field reconnection, *Geophys. Res. Lett.*, *36*, L07102, doi:10.1029/2009GL037463.
- Mozer, F. S., V. Angelopoulos, J. Bonnell, K. H. Glassmeier, and J. P. McFadden (2008), THEMIS observations of modified Hall fields in asymmetric magnetic field reconnection, *Geophys. Res. Lett.*, *35*, L17S04, doi:10.1029/2007GL033033.
- Murphy, N. A. (2009), Simulation and analysis of magnetic reconnection in a laboratory plasma astrophysics experiment, Ph.D. thesis, Univ. of Wisc.–Madison, Madison.
- Murphy, N. A., and C. R. Sovinec (2008), Global axisymmetric simulations of two-fluid reconnection in an experimentally relevant geometry, *Phys. Plasmas*, *15*, 042313, doi:10.1063/1.2904600.
- Nakajima, R. (1985), The circumstellar gas of Sigma Orionis E, *Astrophys. Space Sci.*, *116*, 285–297, doi:10.1007/BF00653783.
- Nakamura, M., and M. Scholer (2000), Structure of the magnetopause reconnection layer and of flux transfer events: Ion kinetic effects, *J. Geophys. Res.*, *105*, 23,179–23,192, doi:10.1029/2000JA900101.
- Nakamura, T. K. M., M. Fujimoto, and H. Sekiya (2010), Interaction of multiple magnetic islands in a long current sheet: Two-fluid simulations, *Geophys. Res. Lett.*, *37*, L02103, doi:10.1029/2009GL041858.
- Øieroset, M., T. D. Phan, and M. Fujimoto (2004), Wind observations of asymmetric magnetic reconnection in the distant magnetotail, *Geophys. Res. Lett.*, *31*, L12801, doi:10.1029/2004GL019958.
- Oka, M., M. Fujimoto, T. K. M. Nakamura, I. Shinohara, and K. Nishikawa (2008), Magnetic reconnection by a self-retreating X line, *Phys. Rev. Lett.*, *101*, 205004, doi:10.1103/PhysRevLett.101.205004.
- Ono, Y., A. Morita, M. Katsurai, and M. Yamada (1993), Experimental investigation of three-dimensional magnetic reconnection by use of two colliding spheromaks, *Phys. Fluids B*, *5*, 3691–3701, doi:10.1063/1.860840.
- Owen, C. J., and S. W. H. Cowley (1987a), Simple models of time-dependent reconnection in a collision-free plasma with an application to substorms in the geomagnetic tail, *Planet. Space Sci.*, *35*, 451–466, doi:10.1016/0032-0633(87)90102-4.
- Owen, C. J., and S. W. H. Cowley (1987b), A note on current sheet stress balance in the geomagnetic tail for asymmetrical tail lobe plasma conditions, *Planet. Space Sci.*, *35*, 467–474, doi:10.1016/0032-0633(87)90103-6.
- Parker, E. N. (1957), Sweet's mechanism for merging magnetic fields in conducting fluids, *J. Geophys. Res.*, *62*, 509–520.
- Parker, E. N. (1963), The solar-flare phenomenon and the theory of reconnection and annihilation of magnetic fields, *Astrophys. J. Suppl.*, *8*, 177–211, doi:10.1086/190087.
- Petrukovich, A. A., W. Baumjohann, R. Nakamura, and H. Rème (2009), Tailward and earthward flow onsets observed by Cluster in a thin current sheet, *J. Geophys. Res.*, *114*, A09203, doi:10.1029/2009JA014064.
- Priest, E., and T. Forbes (2000), *Magnetic Reconnection*, Cambridge Univ. Press, Cambridge, U. K.

- Pritchett, P. L. (2008), Collisionless magnetic reconnection in an asymmetric current sheet, *J. Geophys. Res.*, *113*, A06210, doi:10.1029/2007JA012930.
- Reeves, K. K. (2006), The relationship between flux rope acceleration and thermal energy release in a model of eruptive solar phenomena, *Astrophys. J.*, *644*, 592–597, doi:10.1086/503352.
- Rogers, B., and L. Zakharov (1995), Nonlinear ω_* -stabilization of the $m = 1$ mode in tokamaks, *Phys. Plasmas*, *2*, 3420–3428, doi:10.1063/1.871124.
- Roussev, I., K. Galsgaard, R. Erdélyi, and J. G. Doyle (2001), Modelling of explosive events in the solar transition region in a 2D environment. I. General reconnection jet dynamics, *Astron. Astrophys.*, *370*, 298–310, doi:10.1051/0004-6361:20010207.
- Runov, A., et al. (2003), Current sheet structure near magnetic X-line observed by Cluster, *Geophys. Res. Lett.*, *30*(11), 1579, doi:10.1029/2002GL016730.
- Saint-Hilaire, P., S. Krucker, and R. P. Lin (2009), X-ray emission from the base of a current sheet in the wake of a coronal mass ejection, *Astrophys. J.*, *699*, 245–253, doi:10.1088/0004-637X/699/1/245.
- Schettino, G., G. Poletto, and M. Romoli (2010), CMEs from AR 10365: Morphology and physical parameters of the ejections and of the associated current sheet, *Astrophys. J.*, *708*, 1135–1144, doi:10.1088/0004-637X/708/2/1135.
- Seaton, D. B. (2008), An analysis of reconnection dynamics in an eruptive flare model, Ph.D. thesis, Univ. of N. H., Durham.
- Servidio, S., W. H. Matthaeus, M. A. Shay, P. A. Cassak, and P. Dmitruk (2009), Magnetic reconnection in two-dimensional magnetohydrodynamic turbulence, *Phys. Rev. Lett.*, *102*, 115003, doi:10.1103/PhysRevLett.102.115003.
- Shibata, K., S. Masuda, M. Shimojo, H. Hara, T. Yokoyama, S. Tsuneta, T. Kosugi, and Y. Ogawara (1995), Hot-plasma ejections associated with compact-loop solar flares, *Astrophys. J. Lett.*, *451*, L83–L85, doi:10.1086/309688.
- Shimizu, T., K. Kondo, M. Ugai, and K. Shibata (2009), Magnetohydrodynamics study of three-dimensional fast magnetic reconnection for intermittent snake-like downflows in solar flares, *Astrophys. J.*, *707*, 420–427, doi:10.1088/0004-637X/707/1/420.
- Shiokawa, K., W. Baumjohann, and G. Haerendel (1997), Braking of high-speed flows in the near-Earth tail, *Geophys. Res. Lett.*, *24*, 1179–1182, doi:10.1029/97GL01062.
- Sovinec, C. R., A. H. Glasser, T. A. Gianakon, D. C. Barnes, R. A. Nebel, S. E. Kruger, D. D. Schnack, S. J. Plimpton, A. Tarditi, and M. S. Chu (2004), Nonlinear magnetohydrodynamics simulation using high-order finite elements, *J. Comput. Phys.*, *195*, 355–386, doi:10.1016/j.jcp.2003.10.004.
- Sullivan, B. P., and B. N. Rogers (2008), The scaling of forced collisionless reconnection, *Phys. Plasmas*, *15*(10), 102106, doi:10.1063/1.2992136.
- Sweet, P. A. (1958), The neutral point theory of solar flares, in *Electromagnetic Phenomena in Cosmical Physics, Proceedings of the IAU Symposium*, vol. 6, edited by B. Lehnert, pp. 123–134, Cambridge Univ. Press, London.
- Swisdak, M., B. N. Rogers, J. F. Drake, and M. A. Shay (2003), Diamagnetic suppression of component magnetic reconnection at the magnetopause, *J. Geophys. Res.*, *108*(A5), 1218, doi:10.1029/2002JA009726.
- Tanaka, K. G., et al. (2008), Effects on magnetic reconnection of a density asymmetry across the current sheet, *Ann. Geophys.*, *26*, 2471–2483.
- Townsend, R. H. D., and S. P. Owocki (2005), A rigidly rotating magnetosphere model for circumstellar emission from magnetic OB stars, *Mon. Not. R. Astron. Soc.*, *357*, 251–264, doi:10.1111/j.1365-2966.2005.08642.x.
- ud-Doula, A., R. H. D. Townsend, and S. P. Owocki (2006), Centrifugal breakout of magnetically confined line-driven stellar winds, *Astrophys. J. Lett.*, *640*, L191–L194, doi:10.1086/503382.
- ud-Doula, A., S. P. Owocki, and R. H. D. Townsend (2008), Dynamical simulations of magnetically channelled line-driven stellar winds—II. The effects of field-aligned rotation, *Mon. Not. R. Astron. Soc.*, *385*, 97–108, doi:10.1111/j.1365-2966.2008.12840.x.
- Vršnak, B., et al. (2009), Morphology and density structure of post-CME current sheets, *Astron. Astrophys.*, *499*, 905–916, doi:10.1051/0004-6361/200810844.
- Wang, T., L. Sui, and J. Qiu (2007), Direct observation of high-speed plasma outflows produced by magnetic reconnection in solar impulsive events, *Astrophys. J. Lett.*, *661*, L207–L210, doi:10.1086/519004.
- Wilkinson, J. H. (1959), The evaluation of the zeros of ill-conditioned polynomials. Part I, *Numer. Math.*, *1*, 150–166, doi:10.1007/BF01386381.
- Xing, X., L. R. Lyons, V. Angelopoulos, D. Larson, C. Carlson, A. Runov, and U. Auster (2010), Plasma sheet pressure evolution related to substorms, *J. Geophys. Res.*, *115*, A01212, doi:10.1029/2009JA014315.
- Yamada, M., H. Ji, S. Hsu, T. Carter, R. Kulsrud, N. Bretz, F. Jobes, Y. Ono, and F. Perkins (1997), Study of driven magnetic reconnection in a laboratory plasma, *Phys. Plasmas*, *4*, 1936–1944, doi:10.1063/1.872336.
- Zhu, P., J. Raeder, K. Germaschewski, and C. C. Hegna (2009), Initiation of ballooning instability in the near-Earth plasma sheet prior to the 23 March 2007 THEMIS substorm expansion onset, *Ann. Geophys.*, *27*, 1129–1138.

P. A. Cassak, Department of Physics, West Virginia University, Hodges Hall, Box 6315, Morgantown, WV 26506, USA.
 N. A. Murphy, Harvard-Smithsonian Center for Astrophysics, 60 Garden St., MS 16, Cambridge, MA 02138, USA. (namurphy@cfa.harvard.edu)
 C. R. Sovinec, Department of Engineering Physics, University of Wisconsin–Madison, 1500 Engineering Dr., Madison, WI 53706, USA.